ELSEVIER

Journal of Nuclear Materials 275 (1999) 151–157

journal of nuclear materials

www.elsevier.nl/locate/jnucmat

Equilibrium phase relations in the U–Zr–Fe ternary system

Kinya Nakamura [a], Masaki Kurata [a], Takanari Ogata [a,*], Akinori Itoh [b], Mitsuo Akabori [b]

[a] *Nuclear Fuel Cycle Department, Central Research Institute of Electric Power Industry, Iwato-kita 2-11-1, Komae-shi, Tokyo 201-8511, Japan*

[b] *Japan Atomic Energy Research Institute, Tokai-mura, Ibaraki-ken 319-1195, Japan*

Received 14 January 1999; accepted 10 April 1999

Abstract

Equilibrium phase relations in the U–Zr–Fe ternary system have been investigated experimentally at 853, 973 and 1073 K. The composition of each phase has been determined using the electron probe microanalysis. The differential thermal analysis has also been applied to check the phase relations and examine the stabilities of the ternary compounds. The compositions of the phases found near the sub-binary edges are consistent with the published binary phase diagrams. Three ternary compounds have been found and designated ε, λ and χ, the compositions of which are U–(33–50)Zr–33Fe, U–(21–25)Zr–6Fe and U–32Zr–50Fe (at.%), respectively. The single ε-phase melts at 1206 ± 5 K. The λ-phase decomposes to ε and γ at 999 ± 2 K. The χ-phase exists up to 1168 ± 10 K at the lowest. The equilibrium phase diagrams determined or estimated from the experimental results are consistent with the diagrams calculated using thermodynamic models.

PACS: 81.30.Bx; 64.70.Kb; 64.70.Dv

1. Introduction

A metallic U–Pu–Zr alloy fuel has been recognized as a candidate for advanced fast reactor fuels. One of the key issues in the design of the metallic fuel is the compatibility of the fuel alloy with the Fe-base cladding materials. During irradiation, the fuel alloy swells and comes into contact with the cladding, then metallurgical reactions occur at the fuel alloy–cladding interface. In order to investigate mechanisms of these reactions, it is necessary to prepare fundamental phase diagrams related to the fuel alloy–cladding system. Although the U–Zr–Fe alloy is one of the relevant fundamental systems, only a few studies [1–3] of this alloy have been conducted until now.

In the present study, the U–Zr–Fe alloy samples annealed at 853, 973 and 1073 K have been examined to obtain the equilibrium phase relations in the U–Zr–Fe system. The compositions of the phases formed in the samples have been measured using the electron probe micro-analysis. The differential thermal analysis has been also applied to check the phase relations and examine the stabilities of the ternary compounds. The U–Zr–Fe isotherms obtained experimentally have been compared with the phase diagrams calculated using thermodynamic models.

2. Experimental methods

2.1. Alloy preparation

The U–Zr–Fe alloys were prepared from the pure metals of U (99.9% purity), Zr (99.9%) and Fe (99.995%) by arc-melting in a highly purified argon atmosphere on a water-cooled copper hearth. The arc-melted ingots were inverted and re-melted; the inverting–melting cycle was repeated six times to enhance the homogeneity. Oxidation of the ingots during the fabrication process

* Corresponding author. Tel.: +81-3 3480 2111; fax: +81-3 3480 7956; e-mail: pogata@criepi.denken.or.jp

0022-3115/99/$ - see front matter
PII: S0022-3115(99)00116-6

Table 1
Compositions of U–Zr–Fe alloy ingots fabricated in the study

Alloy No.	Composition (at.%)		
	U	Zr	Fe
1	79.0	11.0	10.0
2	36.0	53.0	11.0
3	46.0	12.0	42.0
4	44.0	25.0	31.0
5	64.0	24.0	12.0
6	72.0	25.0	3.0
7	12.0	74.8	13.2
8	13.0	46.1	40.9
9	16.9	59.0	24.1
10	8.1	65.1	26.7
11	66.3	26.3	7.4
12	23.0	43.6	33.4
13	17.3	33.3	49.5
14	14.3	15.5	70.3
15	31.6	22.3	46.1
16	16.6	37.5	45.9
17	14.5	50.9	34.6

was minimized by arc-melting a pure Zr button before each melting cycle. The C, N and O contents in the final products were less than 190, 60 and 240 ppm, respectively. Compositions of the U–Zr–Fe alloy ingots are summarized in Table 1 and plotted in Fig. 1.

2.2. Phase observation and composition measurement

Three samples of approximately 3 mm × 3 mm × 3 mm were taken from each alloy ingot. Each of the samples was wrapped with tungsten foil, then encapsulated in a quartz tube under an atmosphere of 0.025 MPa helium. The three samples from the same ingot were annealed isothermally at 853, 973 and 1073 K, respectively. Table 2 summarizes the annealing times, which were varied depending on the solidus temperature expected for each alloy and the annealing temperature. After annealing the sample, the capsule was taken out of the furnace and quickly broken in a water bath so that the alloy sample could be quenched rapidly. The annealed sample surface was ground and polished for the electron probe micro-analysis (EPMA). The phases formed in the alloy were observed through back-scattered electron images. The phase compositions were measured using a wave-length dispersive detector. The intensities of U-Mα (0.3910 nm), Zr-Lα (0.6071 nm) and Fe-Kα (0.1936 nm) X-rays were converted to atomic fractions by the ZAF correction.

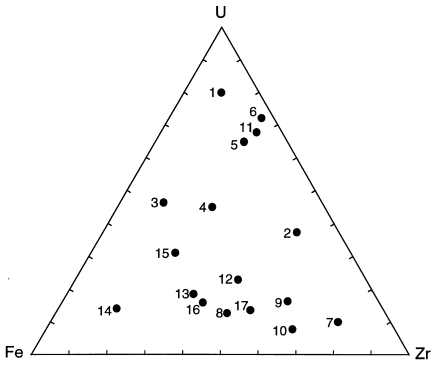

Fig. 1. Plots of compositions of U–Zr–Fe alloy ingots fabricated in the study.

Table 2
Annealing times for U–Zr–Fe alloy samples

Alloy No.	Annealing times (days)		
	853 K	973 K	1073 K
1	180	27	6
2	180	71	12
3	180	71	6
4	180	27	6
5	180	21	12
6	180	21	12
7	170	27	30
8	170	71	30
9	180	71	30
10	170	27	30
11	180	21	11
12	180	21	11
13	81	86	13
14	81	86	40
15	81	86	13
16	81	86	40
17	81	86	13

2.3. Differential thermal analysis

The samples of 100–400 mg for the differential thermal analysis (DTA) were also taken from the arc-melted ingots. The surface of the DTA sample was thoroughly filed to remove potential oxide scale. The sample was put into the lidded alumina container settled on the sensor head. During the differential temperature measurement, the inside of the DTA furnace was purged with highly purified Ar gas flowing at 50 ml/min. Rates of heating and cooling were pro-

Fig. 2. Back-scattered electron images of annealed alloy samples. (a) No. 1 alloy annealed at 973 K; (b) No. 4 alloy annealed at 973 K; (c) No. 5 alloy annealed at 973 K; (d) No. 15 alloy annealed at 973 K; (e) No. 17 alloy annealed at 973 K; (f) No. 15 alloy annealed at 1073 K.

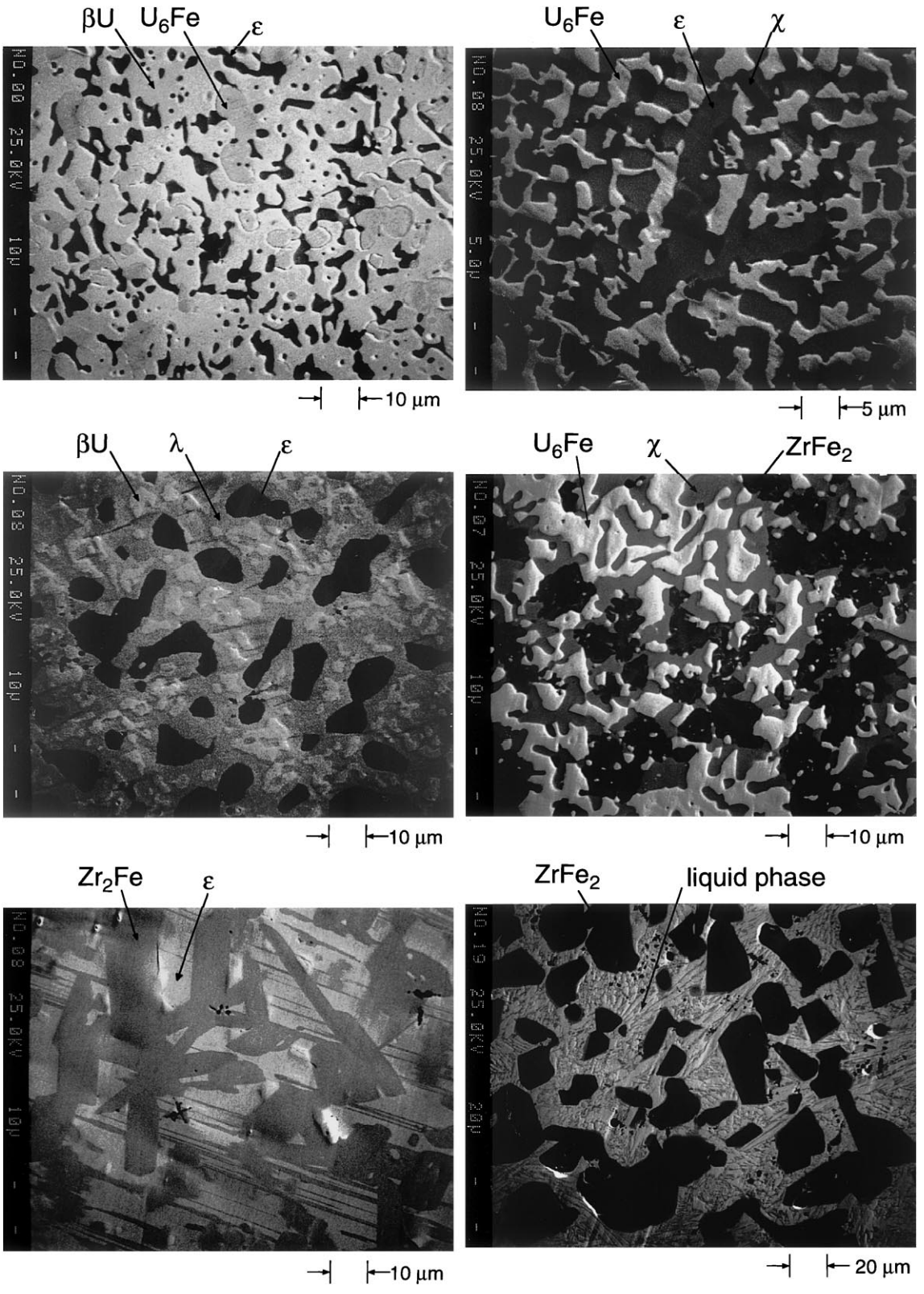
βU
U6Fe
ε
10 μm
U6Fe
ε
χ
5 μm
βU
λ
ε
10 μm
U6Fe
χ
ZrFe2
10 μm
Zr2Fe
ε
10 μm
ZrFe2
liquid phase
20 μm

grammed at 5 and 20 K/min, respectively. The heating–cooling cycles were repeated until reproducibility of the DTA curves was confirmed. After the measurement, weight changes of the samples were negligible and their surfaces remained shiny. This indicates that no excessive sample oxidation occurred during the repeated heating–cooling cycles. The temperatures of the phase transformations have been determined mainly from the heating curves.

3. Results and discussion

3.1. Equilibrium phase relations

Typical back-scattered electron images of the annealed samples are shown in Fig. 2(a)–(f), where the results of the phase identification are also indicated. The equilibrium phase relations obtained from the present experiments at 853, 973 and 1073 K are summarized in Fig. 3(a)–(c), respectively. The thick solid lines in Fig. 3 indicate the boundaries of the three-phase region determined from observation and the composition measurement. In the case that phase compositions could not be quantitatively determined because the phase structure is too minute, the phase relations have been estimated from the phase diagrams of the sub-binary system and/or the results obtained for other ternary samples. The DTA results summarized in Table 3 have also been used to estimate or check the phase relations, and vice versa. The estimated phase relations are indicated by the thick dotted lines in Fig. 3. The thin dotted lines indicate the boundaries of possible single-phase regions. The

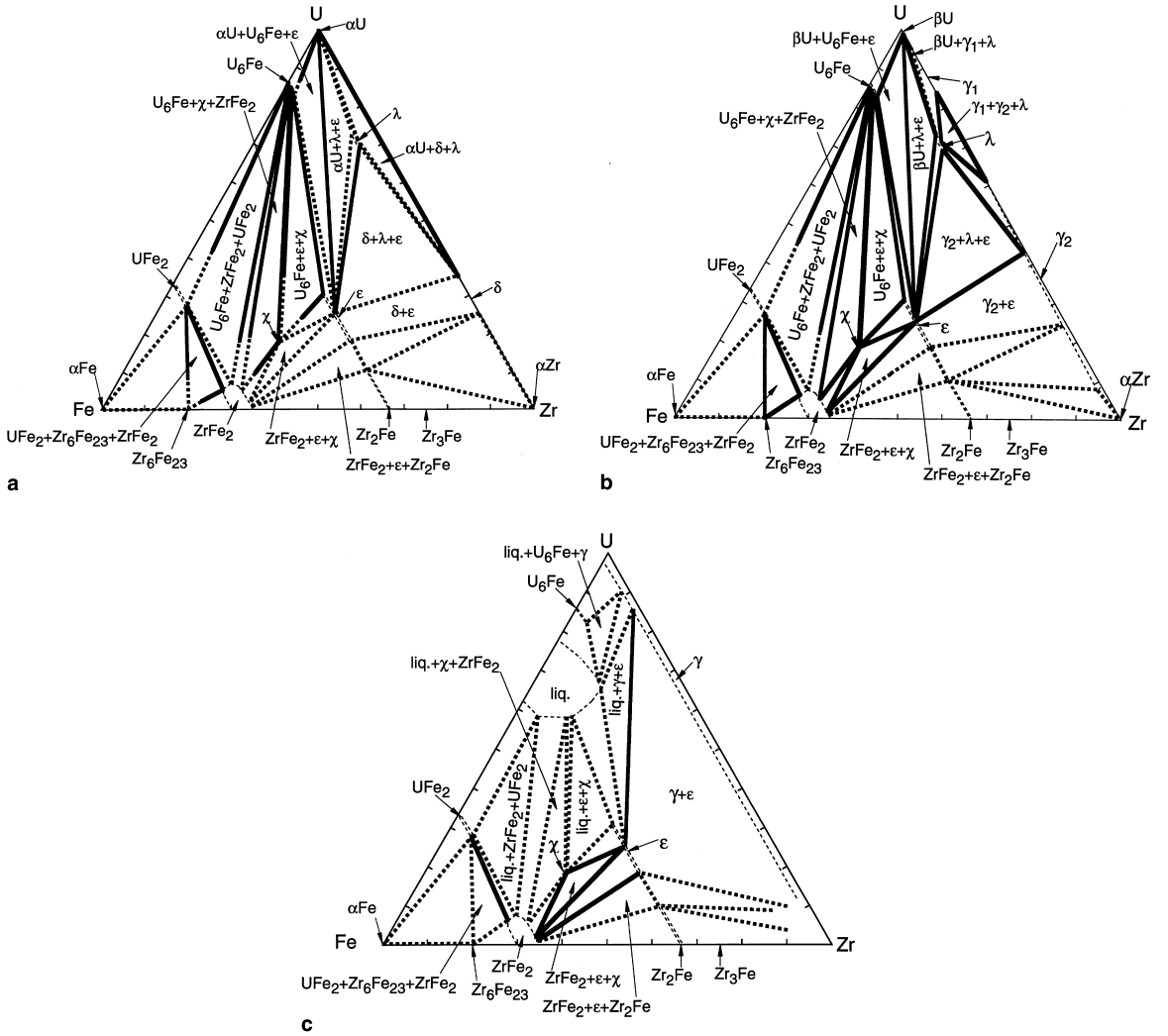

Fig. 3. Equilibrium phase relations experimentally obtained at (a) 853 K; (b) 973 K and (c) 1073 K.

Table 3
Identified phase transformations in U–Zr–Fe alloys

Alloy No.	Temperature (K)	Identified phase transformation
1	944	$\alpha U + U_6Fe + \varepsilon \rightarrow \beta U + U_6Fe + \varepsilon$
	989–996	$\beta U + U_6Fe + \varepsilon \rightarrow \gamma + U_6Fe + \varepsilon$
	1057	$\gamma + U_6Fe + \varepsilon \rightarrow L + \gamma + U_6Fe$
	1082	$L + \gamma + U_6Fe \rightarrow L + \gamma$
	1283 ± 10	$L + \gamma \rightarrow L$
2	880	$\varepsilon + \lambda + \delta \rightarrow \varepsilon + \lambda + \gamma$
	972	$\varepsilon + \lambda + \gamma \rightarrow \varepsilon + \gamma$
	1125	$\varepsilon + \gamma \rightarrow L + \gamma$
	1678 ± 10	$L + \gamma \rightarrow L$
3	995	$U_6Fe + UFe_2 + ZrFe_2 \rightarrow L + ZrFe_2$
	1273 ± 10	$L + ZrFe_2 \rightarrow L$
4	1041	$U_6Fe + \varepsilon + \chi \rightarrow L + \varepsilon$
	1133 ± 10	$L + \varepsilon \rightarrow L$
5	956	$\alpha U + \lambda + \varepsilon \rightarrow \beta U + \lambda + \varepsilon$
	973	$\beta U + \lambda + \varepsilon \rightarrow \gamma + \lambda + \varepsilon$
	998	$\gamma + \lambda + \varepsilon \rightarrow \gamma + \varepsilon$
	1091	$\gamma + \varepsilon \rightarrow L + \gamma$
	1373 ± 10	$L + \gamma \rightarrow L$
6	876	$\alpha U + \lambda + \delta \rightarrow \alpha U + \lambda + \gamma$
	955	$\alpha U + \lambda + \gamma \rightarrow \lambda + \gamma_1 + \gamma_2$
	1001	$\lambda + \gamma_1 + \gamma_2 \rightarrow \varepsilon + \gamma$
	1098	$\varepsilon + \gamma \rightarrow L + \gamma$
	1593 ± 10	$L + \gamma \rightarrow L$
7	878	$Zr_2Fe + \delta + \alpha Zr \rightarrow Zr_2Fe + \gamma$
	1165	$Zr_2Fe + \gamma \rightarrow L + \gamma$
	1723 ± 10	$L + \gamma \rightarrow L$
8	1153	$\varepsilon + Zr_2Fe + ZrFe_2 \rightarrow L + ZrFe_2$
	1221 ± 10	$L + ZrFe_2 \rightarrow L$
9	872	$\varepsilon + Zr_2Fe + \delta \rightarrow \varepsilon + Zr_2Fe + \gamma$
	973–1073	$\varepsilon + Zr_2Fe + \gamma \rightarrow \varepsilon + \gamma$
	1165	$\varepsilon + \gamma \rightarrow L + \gamma$
	1219 ± 5	$L + \gamma \rightarrow L$
10	868	$Zr_2Fe + \delta + \alpha Zr \rightarrow Zr_2Fe + \alpha Zr$
	1053	$Zr_2Fe + \alpha Zr \rightarrow Zr_2Fe + \gamma$
	1165	$Zr_2Fe + \gamma \rightarrow L + Zr_2Fe$
	1333 ± 10	$L + Zr_2Fe \rightarrow L$
11	955	$\alpha U + \varepsilon + \lambda \rightarrow \beta U + \varepsilon + \lambda$
	999	$\beta U + \varepsilon + \lambda \rightarrow \varepsilon + \gamma$
	1102	$\varepsilon + \gamma \rightarrow L + \gamma$
	1573 ± 10	$L + \gamma \rightarrow L$
12	1041	$\varepsilon + \chi \rightarrow L + \varepsilon$
	1206 ± 5	$L + \varepsilon \rightarrow L$
13	1140	$\varepsilon + \chi \rightarrow L + \chi$
	1168 ± 10	$L + \chi \rightarrow L$
14		Not identified
15	994	$U_6Fe + ZrFe_2 + \chi \rightarrow L + ZrFe_2 + \chi$
	1122	$L + ZrFe_2 + \chi \rightarrow L + ZrFe_2$
	1473 ± 10	$L + ZrFe_2 \rightarrow L$
16	1153	$\varepsilon + \chi + ZrFe_2 \rightarrow L + ZrFe_2$
	1195 ± 10	$L + ZrFe_2 \rightarrow L$
17	1193	$\varepsilon + Zr_2Fe \rightarrow L + \varepsilon + Zr_2Fe$
	1228	$L + \varepsilon + Zr_2Fe \rightarrow L + Zr_2Fe$
	1273 ± 10	$L + Zr_2Fe \rightarrow L$

compositions of the phases found near the sub-binary edges are consistent with the published binary phase diagrams [1,4].

The ternary compound having a composition of U–(33–50)Zr–33Fe (at.%) has been found in the U–Zr–Fe system. It can be considered as the same compounds as the ε-phase reported in Ref. [3]. The identification of two other ternary compounds is original to the present study. These compounds have been named λ and χ, the compositions of which are U–(21–25)Zr–6Fe and U–32Zr–50Fe, respectively. Phase relations among the ternary compounds and the other U- or Fe-rich phases are well established, especially at 973 K, as shown in Fig. 3. The stabilities of these ternary compounds are summarized in the subsequent section.

Differences between the phase relations at 853 K (Fig. 3(a)) and 973 K (Fig. 3(b)) are found only along the U–Zr edge, and attributed simply to the transformation of the U–Zr binary system. In the isotherm at 1073 K (Fig. 3(c)), the λ-phase disappears and the liquid phase emerges. The liquid phase boundary in the isotherm at 1073 K has been estimated based on the optimized U–Fe diagrams [1], the isothermal section at 1073 K in the U–Zr–Fe system proposed in Ref. [3], the liquid phase compositions evaluated for Nos. 4 and 15 alloys and the preliminary DTA result. The liquid phase compositions in Nos. 4 and 15 samples have been evaluated by analyzing the area fractions of the liquid phase in their back-scattered electron images (e.g. Fig. 2(f) for the No. 15 sample). In the preliminary DTA, pure U metal was added to the No. 4 alloy sample in the alumina container so that the alloy of the average composition of U–15Zr–18Fe was made during repeated heating–cooling cycles. This DTA result showed that the liquidus was 1074 ± 2 K. As a result, the liquid phase boundary has been drawn as shown in Fig. 3(c).

The phase relations near the Zr-corner in the isothermal section at 1073 K could not be determined well.

3.2. Stability of the ternary compounds

The phase transformations in the U–Zr–Fe alloys have been identified as summarized in Table 3 from the DTA results and the phase relations presented in Fig. 3. The stabilities of the ternary compounds, ε, λ, and χ, have been proved from Table 3 as follows.

The No. 12 alloy sample, almost all of which consists of the ε-phase below 1073 K, shows the liquidus of 1206 ± 5 K. This suggests that the single ε-phase melts at 1206 ± 5 K. The Nos. 5, 6, and 11 samples include the λ-phase, and show phase transformation at 999 ± 2 K. Considering the isotherms shown in Fig. 2, it can be said that the λ-phase decomposes to ε and γ at 999 ± 2 K.

The No. 13 sample consisting of the χ-phase and small amount of the ε-phase below 1073 K shows the liquidus of 1168 ± 10 K, which means that the χ-phase exists up to 1168 ± 10 K at the lowest.

3.3. Comparison with calculated isothermal phase diagrams

Kurata et al. [1] reported the results of the thermodynamic assessment of the U–Zr–Fe system. They optimized the phase diagrams of the U–Fe and U–Zr binary systems using the thermochemical quantities as well as the published phase boundary data, then assessed the U–Zr–Fe system based on the equilibrium phase relations obtained from the early stage results of the present study. Models for the thermodynamic assessment are described in detail in Ref. [1]. Using the same assessment procedure, the isothermal sections at 853, 973 and 1073 K have been calculated again, and are shown in Fig. 4. In the calculation, the ε-phase has been assumed to be a stoichiometric compound for simplicity. Also, the solubilities of Zr in UFe_2, U in $ZrFe_2$ and Zr in U_6Fe have been ignored. The existence of the χ-phase, which had not been found when the previous calculation [1] was carried out, has been incorporated into the present calculation. When Fig. 4 is compared with Fig. 3, some discrepancies can be found near the Zr corner. It is possible that this is because the annealing times for the high-Zr alloy samples (Nos. 7, 9 and 10) were still too short to attain an equilibrium state. Except for the Zr corner, the calculation can reasonably reproduce the phase relations shown in Fig. 3. This means that the phase relations determined or estimated from the present experiment are consistent

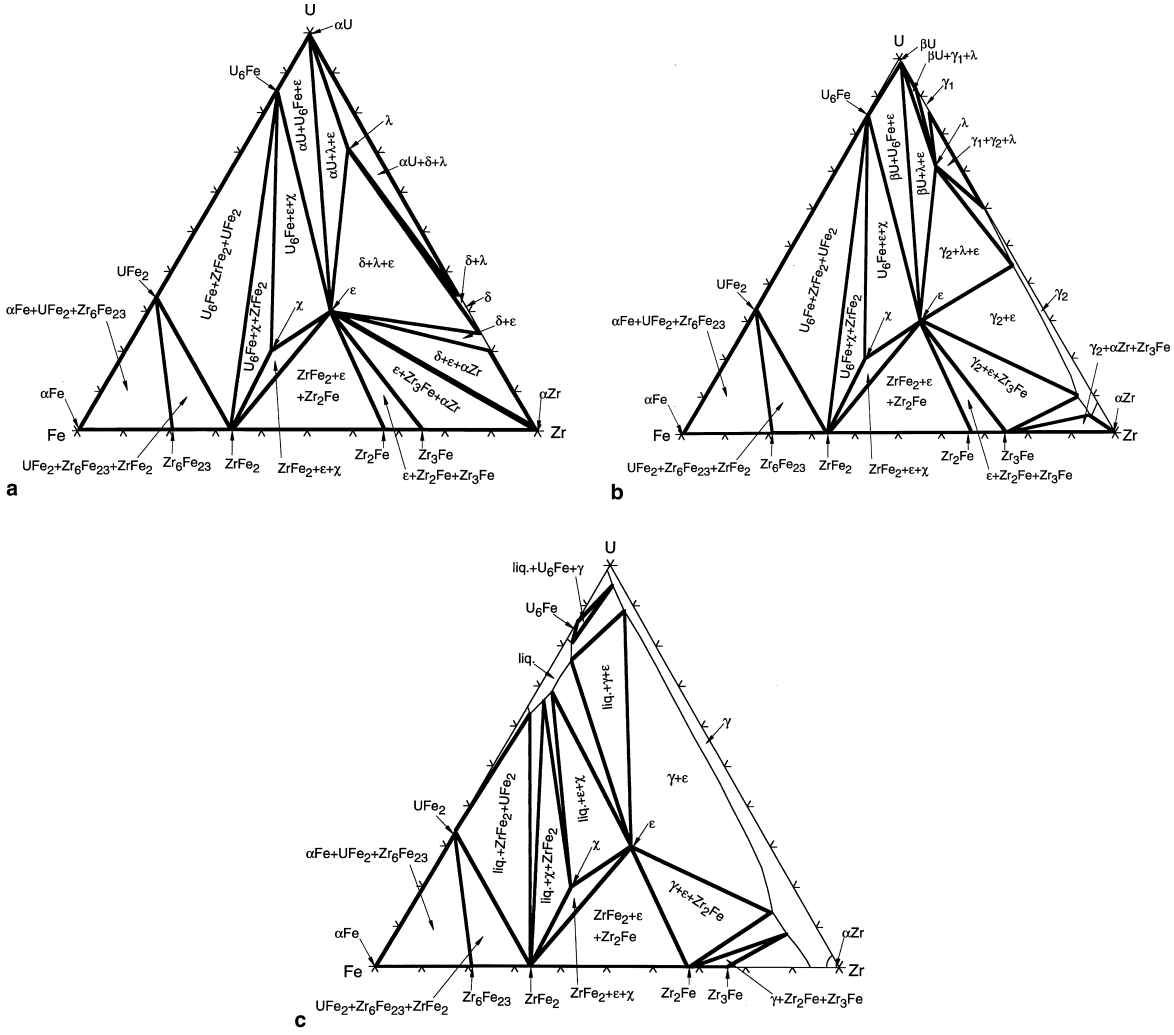

Fig. 4. Calculated U–Zr–Fe ternary isothermal sections at (a) 853 K; (b) 973 K and (c) 1073 K.

with each other and reasonable from a viewpoint of thermodynamics.

4. Conclusion

Equilibrium phase relations in the U–Zr–Fe ternary system have been examined at 853, 973 and 1073 K using EPMA and DTA. The compositions of the phases found near the sub-binary edges are consistent with published binary phase diagrams. Three ternary compounds, ε, λ and χ, have been found and their compositions are U–(33–50)Zr–33Fe, U–(21–25)Zr–6Fe and U–32Zr–50Fe (at.%), respectively. The single ε-phase melts at 1206 ± 5 K. The λ-phase decomposes to ε and γ at 999 ± 2 K. The χ-phase exists up to 1168 ± 10 K at the lowest. The equilibrium phase diagrams determined or estimated from the experimental results are consistent with the diagrams calculated using thermodynamic models.

Acknowledgements

The authors appreciate valuable discussions with Dr T. Ogawa of the Japan Atomic Energy Research Institute and Mr T. Yokoo of the Central Research Institute of Electric Power Industry.

References

[1] M. Kurata, T. Ogata, K. Nakamura, T. Ogawa, J. Alloys Comp. 271–273 (1998) 636.
[2] A.D. Pelton, P.K. Talley, L. Leibowitz, R.A. Blomquist, J. Nucl. Mater 210 (1994) 324.
[3] Annual Progress Report for 1965, Metallurgy Division, Argonne National Laboratory Report ANL-7155.
[4] C. Servant, C. Gueneau, I. Ansara, J. Alloys Comp. 220 (1995) 19.